Water-Assisted Ion Conduction in Solid-State Charge-Transfer Complex Electrolytes for Lithium Batteries

Lingyu Yang[1] and Jennifer L. Schaefer[1]*

[1]Department of Chemical and Biomolecular Engineering, University of Notre Dame, Notre Dame, Indiana 46556
*Jennifer.L.Schaefer.43@nd.edu

Abstract:

Currently, research on solid-state organic electrolytes mainly focuses on polymer electrolytes where ion transport is facilitated by chain segmental motion. A limited number of prior reports suggest that solid-state electrolytes based on organic charge-transfer (CT) complexes can have surprisingly high ionic conductivity. Here, we report that processing and environmental conditions drastically impact charge transport properties of CT complex electrolytes based on tetrathiafulvalene-tetracyanoquinodimethane (TTF-TCNQ) mixed with lithium bis(trifluoromethylsulfonylimide) (LiTFSI). Thermal annealing and water vapor treatment decreases electronic conductivity and increases ionic conductivity. The electrolyte with 1-1-2-0.45 molar ratio of TTF-TCNQ-LiTFSI-H_2O has an ionic conductivity of 2×10^{-3} S/cm at 25 °C with order 10^4 times lower electronic conductivity. In this system where ion conduction is decoupled from the mobility of the organic phase, thermal annealing helps reduce CT connectivity and expose more surfaces to interact with LiTFSI, and water promotes the dissociation of LiTFSI.

TOC Graphic:

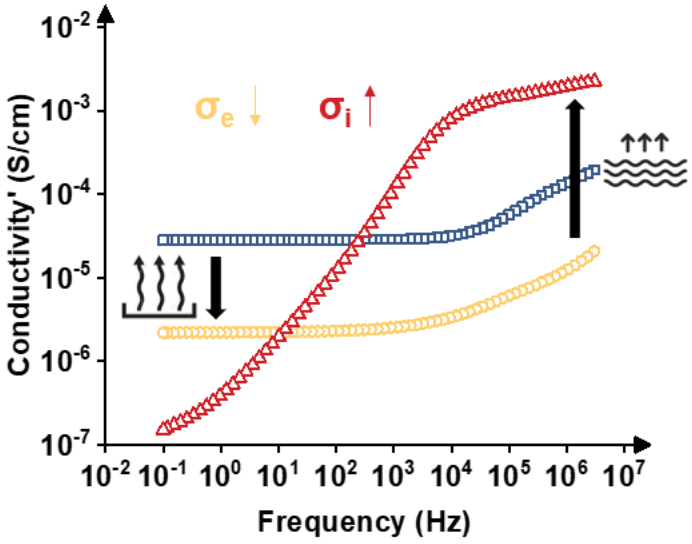

Lithium-ion batteries are widely used in various applications. However, the safety risks due to combustible organic liquid electrolytes have led to significant interest in solid-state electrolytes.[1,2] While inorganic solid electrolytes can have comparable or even higher conductivity than liquid electrolytes,[3] their low mechanical flexibility presents a challenge for commercialization. Despite the lower thermal stability, solid organic electrolytes have the potential advantage of flexibility, providing greater durability to withstand volume changes during cycling.[4] Solid-state polymer electrolytes such as those based on poly(ethylene oxide) have been a focus of much attention, as the polar polymers can bind with Li^+, enable the lithium salt dissociation, and facilitate the transport of Li^+ through the amorphous matrix via polymer segmental motion.[5] However, the conductivity of these polar polymer electrolytes is typically low at room temperature, which has led to the exploration of compounds with lower glass-transition temperatures (Tg).[6] The operating temperature of batteries with solid polymer electrolytes is usually elevated to improve conductivity. Efforts to decouple ion conduction from polymer segmental motion have met limited success, and there are few examples of solid-state polymer electrolytes with ionic conductivity above 10^{-3} S/cm at room temperature.[7,8]

The concept of using charge-transfer (CT) polymer materials as battery electrolytes was first introduced in the patent literature.[9] The three-part combination of polymer with electron-donating groups, small-molecule organic electron acceptors, and lithium salt was reported to achieve surprisingly high ionic conductivity (10^{-4} S/cm at room temperature). Later, Oyaizu and coworkers reported that an array of small-molecule charge-transfer complexes mixed with lithium salt also exhibited elevated ionic conductivity (10^{-6} to 10^{-4} S/cm at room temperature).[10] The authors hypothesized that fast ion transport occurs at the interfaces between the charge-transfer crystals and salt. We are not aware of further reports on these materials. Organic charge-transfer complexes have been studied as fast electronic conductors for five decades while their potential for use in practical electrolytes, where low electronic conductivity is necessary to prevent self-discharge, is unknown.[11–14]

Investigating this phenomenon using the classic charge-transfer complex of tetrathiofulvlene (TTF) and 7,7,8,8-tetracyanoquinodimethane (TCNQ), we found the materials have limited thermal stability so that the composition could not be reliably controlled using melt combination at high temperatures (**Figure S1 and S2**).[10] We adopted a low-temperature, solution-based mixing procedure for creating CT complex electrolytes of TTF-TCNQ with the lithium bis(trifluoromethylsulfonylimide) (LiTFSI) at various ratios (TTF-TCNQ-LiTFSI = 1-1-x, x = 0.5, 1, 1.5, and 2) (**Figure 1a**).[15] Thermal gravimetric analysis shows that these mixtures are thermally stable up to about 150 °C (**Figure S3**).

As CT complexes are electronic conductors while sufficient ionic conduction and low electronic conduction are needed for a successful electrolyte, the nature of the mixed conduction was investigated using both electrochemical impedance spectroscopy (EIS; an alternating current, AC, method) and direct current (DC) polarization on the materials contained in symmetric stainless steel cells.[16] This setup was blocking for ions but not electrons at the electrolyte-electrode interface (**Figure 1b**). The frequency-dependent portrayal of the impedance data reveals constant values of the real conductivity (σ') at frequencies between 10^4 and 10^{-1} Hz at 25 °C for both pure CT complex and the mixtures, which is characteristic of electronic-dominated conduction (**Figure 1c**). The DC polarization method further helped to confirm that only electronic conduction was visible, as the current response is time-independent at each potential step with no current spike and subsequent decay at each step even with the highest concentration of LiTFSI (**Figure 1d)**. The electronic conductivity values extrapolated from the DC polarization method (see **Figure S5**) were similar to the plateau value of the AC profiles. The mixtures showed Arrhenius temperature-dependent electronic conductivity in the range of relationship -20 to

115 °C, with the electronic conductivity decreasing as the doping content of the Li salt increased (**Figure 1e)**. Material characterizations of these fresh mixtures are appended in **Figures S6-7**.[17–23]

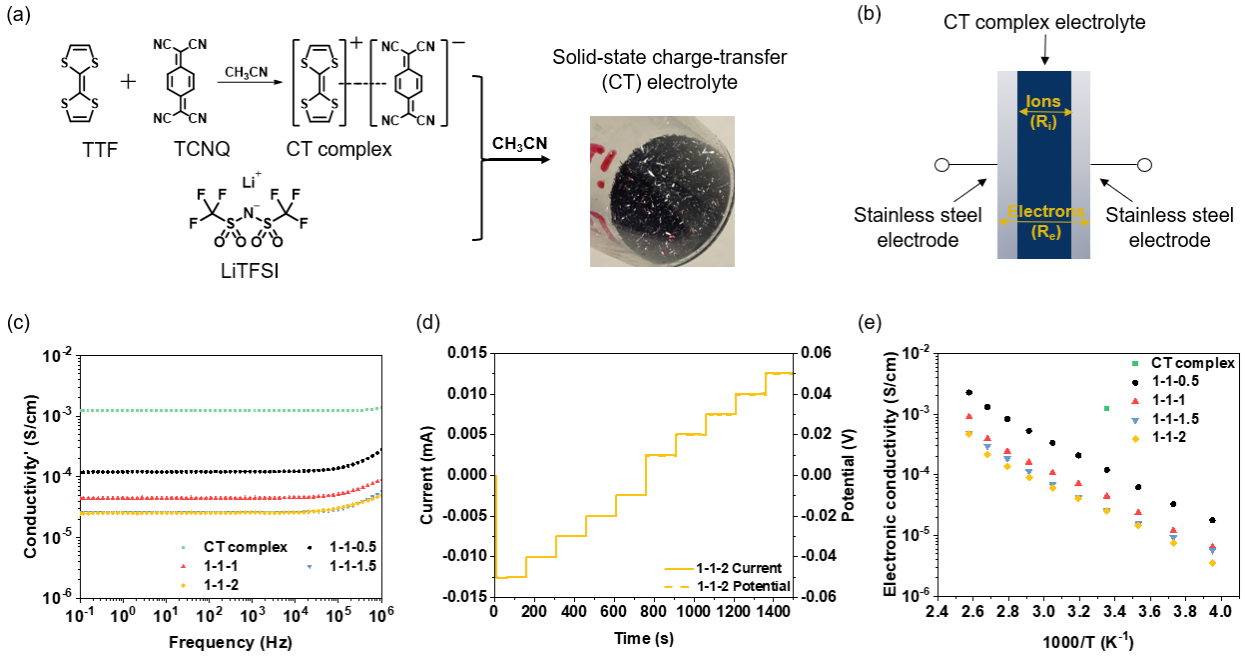

Figure 1. (a) The fabrication of solid-state CT complex electrolytes. (b) Coin cell configuration that was applied to investigate ionic and electronic conduction in the CT complex electrolytes. (c) Frequency-dependent real conductivity profiles from AC measurement of fresh-state mixtures and pure CT complex at 25 °C. (d) Current profile from DC stepwise potentiostatic measurement of sample 1-1-2 at 25 °C. (e) The electronic conductivity as a function of temperature of the samples at the fresh state.

Continued testing in our lab revealed that the electronic conductivity of all the mixtures decreased unpredictably while running cyclic temperature-dependent measurements up to 130 °C. It was also observed in **Figure 1e** that the electronic conductivities at 115 °C exceeded that of the Arrhenius extrapolation from the lower temperature data, and endothermic peaks are observed in differential scanning calorimetry (DSC) scans (**Figure S4**). To understand the impact of high temperature, a thermal annealing process was carried out at 130 °C for 30 minutes. The annealing caused a drop in electronic conductivity. Afterwards, the room-temperature AC conductivity profiles were observed to change on a daily basis (**Figure 2a**), despite that the coin cells just sat on the benchtop. Most interestingly, the shape of the profiles slowly evolved, with the appearance first of an inflection and then an increased conduction plateau at higher frequency and a decay in the real conductivity at low frequency. These real conductivity profiles for the aged samples have shapes expected for ionic conductors, where real conductivity decreases at low frequency due to charge accumulation at the blocking electrode-electrolyte interface.

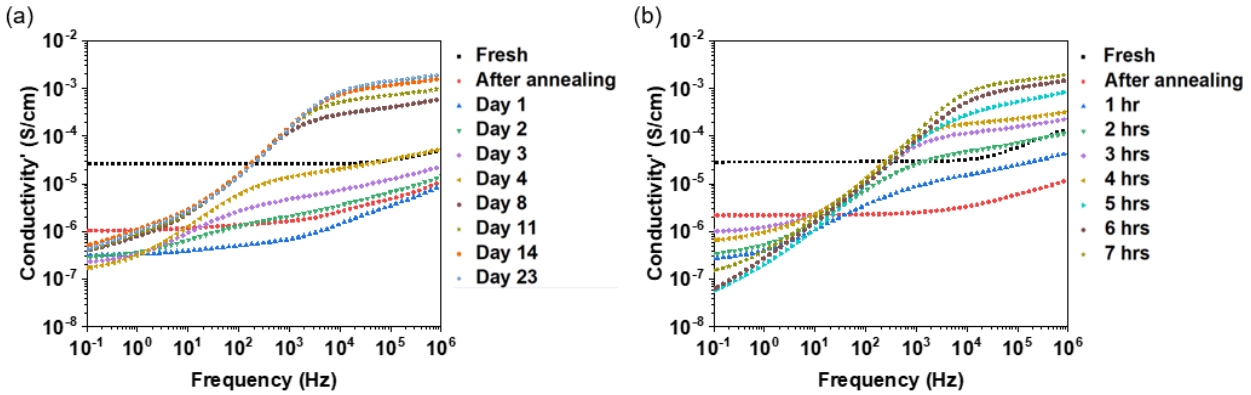

Figure 2. (a) Time-dependent real conductivity profiles at room temperature of electrolyte 1-1-2 in ambient air. (b) Time-dependent real conductivity profile at room temperature of electrolyte 1-1-2 upon treatment in the humid atmosphere.

There were concerns that the coin cells were leaking and causing the ionic conductivity enhancement, therefore, a systematic water vapor treatment was conducted to investigate this issue. After undergoing thermal annealing and cooling to room temperature, the coin cells containing electrolytes with different compositions were placed into a wet nitrogen atmosphere chamber with the relative humidity (RH) values of 95-99 % for 7 hrs. It was observed that the conductivity profiles evolved rapidly and in a manner similar to that of the cells sitting on the benchtop (**Figure 2b**). Differences in the impedance responses between **Figure 2** (a) and (b) reflect the typical cell-to-cell variation observed that is attributed to differences in particulate sample packing. Extensive control testing revealed that this conduction phenomenon was achieved only with exposure to water (no impact of O_2) and only when all mixture components were included (both CT complex and LiTFSI) and with thermal annealing (**Figures S8-11**).

All of the electrolytes remained solid after being treated via thermal annealing and water vapor, even when the sample with the highest concentration of LiTFSI (1-1-2) was exposed to ambient air for over 90 days (**Figure 3a**). We note that, in stark contrast, pure LiTFSI that is left on the counter will absorb enough water to turn into a puddle after 1 hr in ambient air with around 26 % RH (**Figure S12**). The water content in the electrolytes that were purposefully treated was determined via the Karl Fischer (KF) titration method to be 0.65 %, 0.81 %, 0.82 %, and 0.83 % by mass for compositions 1-1-0.5 to 1-1-2, respectively.

The morphological changes of the solid electrolytes were observed using scanning electron microscopy (SEM) and energy-dispersive X-ray spectroscopy (EDS). After thermal annealing and water vapor treatment, LiTFSI was more widely distributed compared to its fresh state (**Figure 3c** and **Figure S13f**). For electrolyte 1-1-2, phase segregation occurred, resulting in a CT complex-dominated phase and a LiTFSI-dominated phase with CT complex crystals wrapped by LiTFSI. The texture of the salt phase is notably smoother. We hypothesize that electrons may transport along the TCNQ stack, and lithium cations may transport on the surface of the CT complex along the stack in the opposite direction to electrons. Long range charge transport requires movement from one CT complex surface to another. As suggested by Oyaizu and colleagues, the resistance for electron transport between CT complexes and through the salt phase is likely much higher when the continuous CT crystal phases are separated, hence this is why electronic conduction may be suppressed in some circumstances.[10]

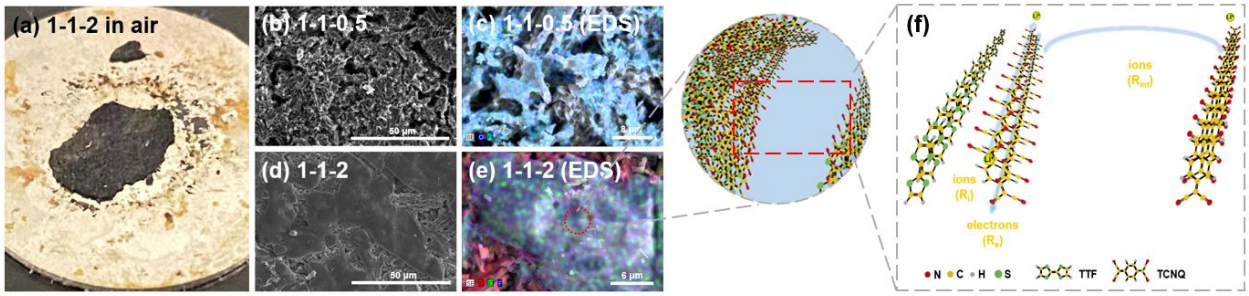

Figure 3. (a) Open coin cell of treated electrolyte 1-1-2 exposed in ambient air for more than 90 days. (b and c) SEM and EDS of treated electrolyte 1-1-0.5. (d and e) SEM and EDS of treated electrolyte 1-1-2. (f) The proposed transport pathways of electrons and ions through the treated CT complex electrolytes.

In such a molecular arrangement (**Figure 3f**), it is appropriate to model the charge transport using an equivalent circuit that incorporates ionic (ionic resistance, R_i) and electronic (electronic resistance, R_e) pathways in parallel. We adopted the equivalent circuit illustrated in **Figure 4a** that is commonly used in the mixed conductors community.[24,25] Here, R_c represents the total contact resistance of the coin cell assembly, and CPE_{dl} and CPE_g are constant phase elements corresponding to the double-layer capacitive property arising from ionic conduction at the electrode/electrolyte interface and geometric capacitance due to the presence of electrolyte with a dielectric constant, respectively. In parallel are the interparticle resistance (R_{int}) and interface constant phase elements (CPE_{int}), where the former represents the resistance arising from the ions transporting from the surface of one CT complex crystal to another, and the latter is attributed to capacitance at the microstructure level.

This equivalent circuit model was able to fit all temperature-dependent EIS results for the treated samples very well (**Figure 4b** and **Figures S14**). The temperature-dependent ionic, electronic, and interparticle conductivities of the treated samples are shown in **Figure 4c-e**. The electronic conductivity decreased order 1000 times after treatment, while the ionic conductivity dominated in the mixed conduction. Ionic conductivities fell in the range of 10^{-5} to 10^{-3} S/cm at 25 °C, with the highest ionic conductivity of 2×10^{-3} S/cm observed for treated electrolyte 1-1-2 . It was observed that the interparticle conductivities varied from 10^{-9} to 10^{-5} S/cm; ionic conduction through the Li salt between CT complexes was not enhanced. To validate the impedance fitting results and choice of equivalent circuit model, DC polarization was applied to measure the pure electronic conductivity at 10, 25, and 40 °C (**Figure S15**). The electronic conductivities extracted from the DC method were within the same order of magnitude but lower than those fitted from the equivalent circuit model, likely due to fitting errors from the limited range of frequency in AC measurements.

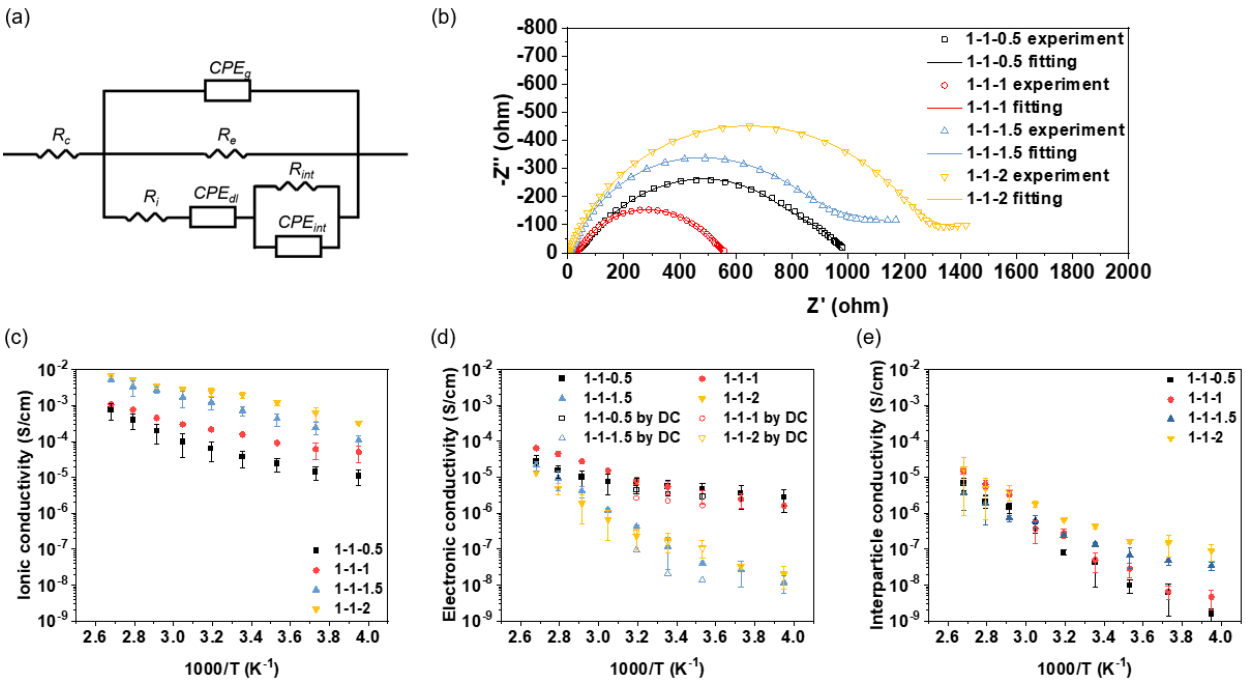

Figure 4. (a) The equivalent circuit model used to fit EIS profiles for the treated electrolytes. (b) The experimental data (points) and equivalent circuit model fitting lines for all four treated electrolytes at 100 °C. (c, d, and e) The temperature-dependent electronic, ionic, and interparticle conductivity of treated electrolytes, respectively.

To deconvolute how thermal annealing and trace amounts of water enhanced the ion transport in the CT-based electrolytes, a series of controlled experiments were performed. The temperature-dependent WAXS profiles of pure CT complex and electrolyte 1-1-2, which were annealed at 130 °C for 30 min (**Figure S16** and **S17**), were analyzed. The average size of the primary CT complex crystallites stayed the same at around 80 nm, as calculated using the Scherrer equation.[26] However, we saw the secondary particles were reduced in size (**Figure S18**), which contributed to the decrease in connectivity between CT crystals and thus in electronic conductivity.[27,28] The WAXS peak positions of electrolyte 1-1-2 remained largely unchanged after thermal annealing, with peak disappearance in two select regions as described in the SI that we attribute to the solvation of LiTFSI by TCNQ. WAXS on water vapor treated samples contained additional peaks attributed to LiTFSI-water complexes (**Figure S19**)[29–32] The state of water and the $TFSI^-$ in the water vapor treated samples were further probed with FTIR (**Figure 5a**). A broad peak emerged at 3300 to 3700 cm^{-1}, which can be assigned to the water molecules donating one or two hydrogen bonds to $TFSI^-$, thus enhancing the dissociation of LiTFSI into the ionic state (**Figure 5b)**.[33] As shown in **Figure 5c**, the peak associated with the S-N stretching mode of $TFSI^-$ at 745 cm^{-1} shifted to 740 cm^{-1} from fresh to treated state of 1-1-2.[34] As the $TFSI^-$ anions dissociate from cations, its stretching peak shifts to lower wavenumbers, so this blue shift happening in electrolyte 1-1-2 represents more free Li^+ and $TFSI^-$ at the treated state.[35]

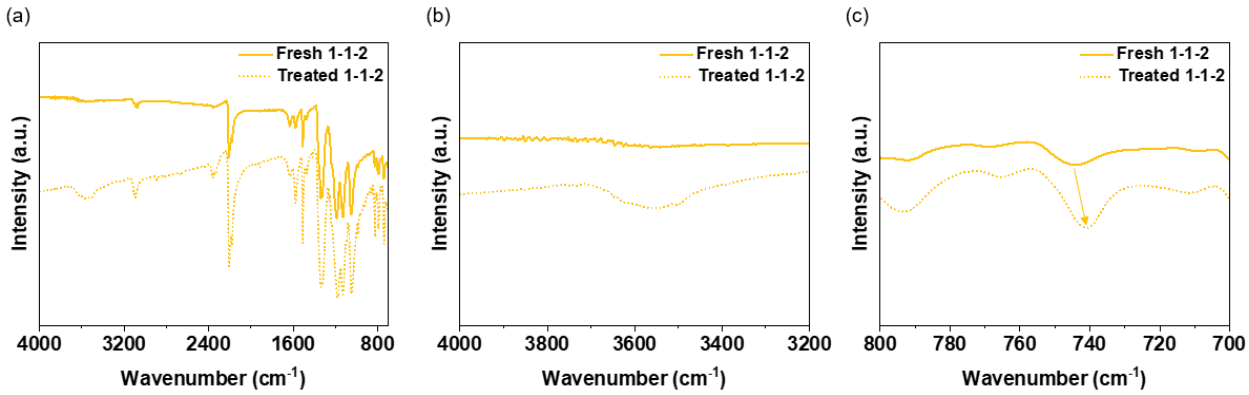

Figure 5. FTIR spectra of both fresh and treated electrolyte 1-1-2 (a) with the zoomed-in range of (b) water and (c) $TFSI^-$. Intensities were rescaled for a better illustration.

In addition, the electrolyte 1-1-2 was purposefully combined with liquid water to investigate if the ionic conduction could be similarly enhanced. Different amounts of water were mixed with dry electrolyte at molalities of 40 and 80 m (concentration of LiTFSI in water). These samples were in the near-solid state, and it was difficult to differentiate the ionic conductivity as electronic (10^{-7} S/cm) and ionic (10^{-6} S/cm) conductivity were comparable (**Figure S9**). In contrast, pure LiTFSI in water (40 and 80 m) had bulk conductivity as low as 10^{-9} S/cm (**Figure S10**). These results suggest that the water vapor treatment results in non-uniform distribution of water in the treated CT-based electrolytes. We hypothesize that water primarily accumulates at the salt - CT complex interface, resulting in some local amorphization of the salt and contributing to ion pair dissociation.

In this study, we demonstrate that trace water facilitates relatively fast ion transport in solid-state electrolytes consisting of organic CT complexes and lithium salt. Total ionic conductivity of 2×10^{-3} S/cm is found at 25 °C for a mixture of 1-1-2-0.45 mole ratio of TTF-TCNQ-LiTFSI-H_2O, corresponding with 250 m of LiTFSI in water. Thermal annealing is found to reduce CT crystal connectivity and electronic conductivity such that the ratio of ionic to electronic conductivity is more than 10^4. The properties of these electrolytes are intriguing given the current understanding in the field of ion conduction mechanisms in the solid state. We propose that the lack of literature and inconsistency of some reports on CT-based electrolytes is due to challenges with electronic conduction and water contamination. The influence of water on the chemical and electrochemical stability of these electrolytes applied in real batteries is still yet to be uncovered, and practical systems require low electronic conductivity to limit self-discharge and promote device lifetime.[36] More research on the molecular level phenomena and its relation to bulk transport and electrochemical properties of these complex electrolytes is warranted.

Notes: The authors report no conflicts of interest.

Acknowledgements: The authors thank the Patrick and Jana Eilers Graduate Student Fellowship and the University of Notre Dame for financial support. The authors thank the ND Center for Environmental Science and Technology for FTIR instrumentation, the ND Integrated Imaging Facility for electron microscopy, Prof. Ruilan Guo for TGA and DSC instrumentation, and Ivan Kuzmenko at APS beamline 12-ID-B for assistance with WAXS measurements. This research used resources of the Advanced Photon Source, a U.S. Department of Energy (DOE) Office of Science User Facility operated for the DOE Office of Science by Argonne National Laboratory under Contract No. DE-AC02-06CH11357. The authors also

gratefully acknowledge the many colleagues that provided feedback and engaged in conversation on this topic at the ACS National Meeting Fall 2022, the 2022 TSRC Workshop: Materials Chemistry in Electrochemical Energy Storage, and the 2022 International Symposium on Polymer Electrolytes.

Supporting Information Available: electrolyte preparation methods, characterization of electrolytes (TGA, DSC, WAXS, FTIR, and SEM), AC and DC conductivity measurements, analysis of Nyquist plots, and results of KF titration

References

(1) Zheng, F.; Kotobuki, M.; Song, S.; Lai, M. O.; Lu, L. Review on Solid Electrolytes for All-Solid-State Lithium-Ion Batteries. *J. Power Sources* **2018**, *389* (February), 198–213. https://doi.org/10.1016/j.jpowsour.2018.04.022.

(2) Janek, J.; Zeier, W. G. A Solid Future for Battery Development. *Nat. Energy* **2016**, *1* (9), 1–4. https://doi.org/10.1038/nenergy.2016.141.

(3) Fergus, J. W. Ceramic and Polymeric Solid Electrolytes for Lithium-Ion Batteries. *Journal of Power Sources*. 2010, pp 4554–4569. https://doi.org/10.1016/j.jpowsour.2010.01.076.

(4) Chen, R.; Qu, W.; Guo, X.; Li, L.; Wu, F. The Pursuit of Solid-State Electrolytes for Lithium Batteries: From Comprehensive Insight to Emerging Horizons. *Mater. Horizons* **2016**, *3* (6), 487–516. https://doi.org/10.1039/C6MH00218H.

(5) Chen, J.; Xiong, J.; Ji, S.; Huo, Y.; Zhao, J.; Liang, L. All Solid Polymer Electrolytes for Lithium Batteries. *Prog. Chem.* **2020**, *32* (4), 481–496. https://doi.org/10.7536/PC190627.

(6) Hatakeyama-Sato, K.; Tezuka, T.; Umeki, M.; Oyaizu, K. AI-Assisted Exploration of Superionic Glass-Type Li+ Conductors with Aromatic Structures. *J. Am. Chem. Soc.* **2020**, *142* (7), 3301–3305. https://doi.org/10.1021/jacs.9b11442.

(7) Wang, Y.; Agapov, A. L.; Fan, F.; Hong, K.; Yu, X.; Mays, J.; Sokolov, A. P. Decoupling of Ionic Transport from Segmental Relaxation in Polymer Electrolytes. *Phys. Rev. Lett.* **2012**, *108* (8), 088303. https://doi.org/10.1103/PhysRevLett.108.088303.

(8) Jones, S. D.; Nguyen, H.; Richardson, P. M.; Chen, Y. Q.; Wyckoff, K. E.; Hawker, C. J.; Clément, R. J.; Fredrickson, G. H.; Segalman, R. A. Design of Polymeric Zwitterionic Solid Electrolytes with Superionic Lithium Transport. *ACS Cent. Sci.* **2022**, *8* (2), 169–175. https://doi.org/10.1021/acscentsci.1c01260.

(9) Zimmerman, M. Solid Ionically Conducting Polymer Material. U.S. Patent US15/2820022016.

(10) Hatakeyama-Sato, K.; Umeki, M.; Tezuka, T.; Oyaizu, K. Charge-Transfer Complexes for Solid-State Li+Conduction. *ACS Appl. Electron. Mater.* **2020**, *2* (7), 2211–2217. https://doi.org/10.1021/acsaelm.0c00393.

(11) Alves, H.; Molinari, A. S.; Xie, H.; Morpurgo, A. F. Metallic Conduction at Organic Charge-Transfer Interfaces. *Nat. Mater.* **2008**, *7* (7), 574–580. https://doi.org/10.1038/nmat2205.

(12) Bryce, M. R.; Petty, M. C. Electrically Conductive Langmuir–Blodgett Films of Charge-Transfer Materials. *Nature* **1995**, *374* (6525), 771–776. https://doi.org/10.1038/374771a0.

(13) Goetz, K. P.; Vermeulen, D.; Payne, M. E.; Kloc, C.; McNeil, L. E.; Jurchescu, O. D. Charge-Transfer Complexes: New Perspectives on an Old Class of Compounds. *J. Mater. Chem. C* **2014**,

2 (17), 3065–3076. https://doi.org/10.1039/c3tc32062f.

(14) Takahashi, Y.; Hayakawa, K.; Naito, T.; Inabe, T. What Happens at the Interface between TTF and TCNQ Crystals (TTF = Tetrathiafulvalene and TCNQ = 7,7,8,8-Tetracyanoquinodimethane)? *J. Phys. Chem. C* **2012**, *116* (1), 700–703. https://doi.org/10.1021/jp2074368.

(15) Wu, L.; Wu, F.; Sun, Q.; Shi, J.; Xie, A.; Zhu, X.; Dong, W. A TTF-TCNQ Complex: An Organic Charge-Transfer System with Extraordinary Electromagnetic Response Behavior. *J. Mater. Chem. C* **2021**, *9* (9), 3316–3323. https://doi.org/10.1039/d0tc05230b.

(16) Rawlings, D.; Lee, D.; Kim, J.; Magdău, I. B.; Pace, G.; Richardson, P. M.; Thomas, E. M.; Danielsen, S. P. O.; Tolbert, S. H.; Miller, T. F.; Seshadri, R.; Segalman, R. A. Li+and Oxidant Addition to Control Ionic and Electronic Conduction in Ionic Liquid-Functionalized Conjugated Polymers. *Chem. Mater.* **2021**, *33* (16), 6464–6474. https://doi.org/10.1021/acs.chemmater.1c01811.

(17) Torrance, J. B. An Overview of Organic Charge-Transfer Solids: Insulators, Metals, and the Neutral-Ionic Transition. *Mol. Cryst. Liq. Cryst.* **1985**, *126* (1), 55–67. https://doi.org/10.1080/15421408508084154.

(18) Ramanathan, R.; Kandjani, A. E.; Walia, S.; Balendhran, S.; Bhargava, S. K.; Kalantar-Zadeh, K.; Bansal, V. 3-D Nanorod Arrays of Metal-Organic KTCNQ Semiconductor on Textiles for Flexible Organic Electronics. *RSC Adv.* **2013**, *3* (39), 17654–17658. https://doi.org/10.1039/c3ra43291b.

(19) Melby, L.R., Harder, R.J., Hertler, W.R., Mahler, W., Benson, R.E. and Mochel, W.E. (1962) Substituted Quinodimethans. II. Anion-Radical Derivatives and Complexes of 7,7,8,8-Tetracyanoquinodimethan. *J. Amer. Chem. Soc.*, **1962**, *84*, 3370-3374. https://doi.org/10.1021/ja00876a028

(20) Iguchi, H.; Furutani, H.; Kimizuka, N. Ionic Charge-Transfer Liquid Crystals Formed by Alternating Supramolecular Copolymerization of Liquid π-Donors and TCNQ. *Front. Chem.* **2021**, *9* (March), 1–12. https://doi.org/10.3389/fchem.2021.657246.

(21) Goudappagouda; Chithiravel, S.; Krishnamoorthy, K.; Gosavi, S. W.; Santhosh Babu, S. Seeded On-Surface Supramolecular Growth for Large Area Conductive Donor-Acceptor Assembly. *Chem. Commun.* **2015**, *51* (52), 10439–10442. https://doi.org/10.1039/c5cc03091a.

(22) Kistenmacher, T. J.; Phillips, T. E.; Cowan, D. O. The Crystal Structure of the 1:1 Radical Cation–Radical Anion Salt of 2,2'-Bis-l,3-Dithiole (TTF) and 7,7,8,8-Tetracyanoquinodimethane (TCNQ). *Acta Crystallogr. Sect. B Struct. Crystallogr. Cryst. Chem.* **1974**, *30* (3), 763–768. https://doi.org/10.1107/s0567740874003669.

(23) Dar, A. A.; Rashid, S. Organic Co-Crystal Semiconductors: A Crystal Engineering Perspective. *CrystEngComm* **2021**, *23* (46), 8007–8026. https://doi.org/10.1039/d1ce01117k.

(24) Huggins, R. A. Simple Method to Determine Electronic Conductivity and Ionic Components of the Conductors in Mixed a Review. *Ionics (Kiel).* **2002**, *8* (3–4), 300–313. https://doi.org/10.1007/BF02376083.

(25) Feig, V. R.; Tran, H.; Lee, M.; Bao, Z. Mechanically Tunable Conductive Interpenetrating Network Hydrogels That Mimic the Elastic Moduli of Biological Tissue. *Nat. Commun.* **2018**, *9* (1), 1–9. https://doi.org/10.1038/s41467-018-05222-4.

(26) Oyama, M.; Wei, Q.; Mukaida, M.; Kawanishi, Y.; Ishida, T. Electrical Conduction and Thermoelectric Properties of Tetrathiafulvalene-Tetracyanoquinodimethane Cast Films Prepared with N,N-Dimethylacetamide. *Synth. Met.* **2017**, *230* (February), 12–17.

https://doi.org/10.1016/j.synthmet.2017.05.013.

(27) Odom, S. A.; Caruso, M. M.; Finke, A. D.; Prokup, A. M.; Ritchey, J. A.; Leonard, J. H.; White, S. R.; Sottos, N. R.; Moore, J. S. Restoration of Conductivity with TTF-TCNQ Charge-Transfer Salts. *Advanced Functional Materials*. 2010, pp 1721–1727. https://doi.org/10.1002/adfm.201000159.

(28) Park, C.; Atalla, V.; Smith, S.; Yoon, M. Understanding the Charge Transfer at the Interface of Electron Donors and Acceptors: TTF–TCNQ as an Example. *ACS Appl. Mater. Interfaces* **2017**, *9* (32), 27266–27272. https://doi.org/10.1021/acsami.7b04148.

(29) Xue, L.; Padgett, C. W.; DesMarteau, D. D.; Pennington, W. T. Synthesis and Structures of Alkali Metal Salts of Bis[(Trifluoromethyl)Sulfonyllimide. *Solid State Sci.* **2002**, *4* (11–12), 1535–1545. https://doi.org/10.1016/S1293-2558(02)00050-X.

(30) Guo, Y.; Terban, M. W.; Moudrakovski, I.; Münchinger, A.; Dinnebier, R. E.; Popovic, J.; Maier, J. Ion Transport in Semi-Solid Water-in-Salt Electrolytes: LiTFSI-H2O as a Model System. *J. Mater. Chem. A* **2023**, 3427–3436. https://doi.org/10.1039/d2ta08047h.

(31) Nowinski, J. L.; Lightfoot, P.; Bruce, P. G. Structure of LiN(CF3SO2)2, a Novel Salt for Electrochemistry. *J. Mater. Chem.* **1994**, *4* (10), 1579–1580. https://doi.org/10.1039/JM9940401579.

(32) Ding, M. S.; Xu, K. Phase Diagram, Conductivity, and Glass Transition of LiTFSI-H2O Binary Electrolytes. *J. Phys. Chem. C* **2018**, *122* (29), 16624–16629. https://doi.org/10.1021/acs.jpcc.8b05193.

(33) Zhang, Y.; Lewis, N. H. C.; Mars, J.; Wan, G.; Weadock, N. J.; Takacs, C. J.; Lukatskaya, M. R.; Steinrück, H. G.; Toney, M. F.; Tokmakoff, A.; Maginn, E. J. Water-in-Salt LiTFSI Aqueous Electrolytes. 1. Liquid Structure from Combined Molecular Dynamics Simulation and Experimental Studies. *J. Phys. Chem. B* **2021**, *125* (17), 4501–4513. https://doi.org/10.1021/acs.jpcb.1c02189.

(34) Kam, W.; Liew, C. W.; Lim, J. Y.; Ramesh, S. Electrical, Structural, and Thermal Studies of Antimony Trioxide-Doped Poly(Acrylic Acid)-Based Composite Polymer Electrolytes. *Ionics (Kiel).* **2014**, *20* (5), 665–674. https://doi.org/10.1007/s11581-013-1012-0.

(35) Park, B.; Andersson, R.; Pate, S. G.; Liu, J.; O'Brien, C. P.; Hernández, G.; Mindemark, J.; Schaefer, J. L. Ion Coordination and Transport in Magnesium Polymer Electrolytes Based on Polyester-Co-Polycarbonate. *Energy Mater. Adv.* **2021**, *2021*. https://doi.org/10.34133/2021/9895403.

(36) Suo, L.; Borodin, O.; Gao, T.; Olguin, M.; Ho, J.; Fan, X.; Luo, C.; Wang, C.; Xu, K. "Water-in-Salt" Electrolyte Enables High-Voltage Aqueous Lithium-Ion Chemistries. *Science (80-.).* **2015**, *350* (6263), 938–943. https://doi.org/10.1126/science.aab1595.

Supporting Information

Materials. Tetrathiafulvalene (TTF, > 99.0%) was purchased from TCI Chemicals. Lithium bis(trifluoromethylsulfonyl)imide (LiTFSI, 98+%) was purchased from Thermo Scientific and dried at 100 °C for 24 hrs before use. 7,7,8,8-Tetracyanoquinodimethane (TCNQ, 98%), potassium iodide (KI, anhydrous, free-flowing, ACS reagent, ≥99%), diethyl ether (anhydrous, ACS reagent, ≥99.0%), and acetonitrile (CH_3CN, anhydrous, 99.8%) were purchased from Sigma-Aldrich. Acetone (ACS grade) and methanol (MeOH, ACS grade) were purchased from VWR international. All chemicals except LiTFSI were used without further purification.

Electrolyte preparation. To fabricate the CT complex, TTF (250 mg, 1.22 mmol) and TCNQ (250 mg, 1.22 mmol) were each dissolved in 100 mL of anhydrous acetonitrile at a concentration of 2.5 mg/ml, separately. Then at 60 °C, the TTF solution was added dropwise to the TCNQ solution over 30 min. After the mixed solution was cooled down to room temperature, the target solid TTF-TCNQ CT complex was obtained by vacuum filtration.[1] The TTF-TCNQ CT complex was transferred into an argon glovebox and dried under vacuum at 75 °C for 24 hrs to remove the remaining solvent. Different molar ratios of LiTFSI dissolved in anhydrous acetonitrile were mixed with the TTF-TCNQ CT complex. After sitting in an open container in the glovebox overnight, most solvent evaporated. Then, the CT complex electrolytes were dried in the vacuum oven in the glovebox at 85 °C for 72 hrs to obtain the solid-state electrolytes. The electrolytes were prepared with the molar ratios of TTF-TCNQ-LiTFSI = 1-1-x (mol/mol/mol), where x = 0.5, 1, 1.5, and 2, respectively.

Synthesis of potassium tetracyanoquinodimethane (KTCNQ). TCNQ (102.82 mg, 5×10^{-4} mol) was dissolved in 10 mL anhydrous CH_3CN, and KI (251.33 mg, 1.5×10^{-3} mol) was dissolved in a mixed solvent (0.5 mL anhydrous CH_3CN, 4.5 mL acetone, and 2 mL MeOH). At 80 °C, boiled KI solution was dripped into the boiled TCNQ solution. Afterwards, the solution was cooled down to room temperature. Purple crystals were collected by vacuum filtration and washed several times with diethyl ether.[2] Then the obtained KTCNQ was dried in the vacuum oven at 70 °C for 20 hrs.

Thermal gravimetric analysis (TGA). Thermogravimetric analysis (TGA) was performed on a TGA Q500 (TA Instruments) from 40 to 400 °C under a 50 mL/min nitrogen atmosphere purge at a heating rate of 5 °C/min.

Differential scanning calorimetry (DSC). The thermal transitions of CT complex electrolytes were monitored by differential scanning calorimetry (DSC) Q2000 (TA Instruments) under a nitrogen purge of 50 mL/min, with a heating/cooling rate of 5 °C/min and isothermal period of 2 min unless otherwise specified.

Coin cell assembly. In the argon glovebox, 2032 type coin cells (MTI Corp) were fabricated with the solid-state electrolyte placed between two stainless steel disks (15.5 mm diameter × 0.2 mm thick) as electrodes within a 100 μm-thick Teflon film ring that served as the spacer to maintain the electrolyte thickness. In such a configuration, the ions were conducted through the electrolyte and blocked at the electrolyte/electrode interface whereas the transport of electrons was not blocked at the interface.

Electrochemical impedance spectroscopy (EIS) / alternating current (AC) measurements. EIS/AC measurements were conducted on a Novocontrol Broadband Dielectric spectrometer equipped with an alpha-A high performance frequency analyzer and Quatro temperature control system with a cryostat. Data was collected on coin cells in a frequency range from 1×10^6 Hz to 0.1 Hz at an AC voltage

amplitude of 0.01 V from -20 to 100 °C, 115 °C, or 130 °C (varied) at intervals of 15 °C. The temperature was ramped at 5 °C/min with 5 min of stabilization time at each measurement temperature.

Electronic conductivity measurements (DC polarization method). All DC conductivity measurements were performed using a PARSTAT MC1000 (Princeton Applied Research) potentiostat. The voltage was increased in a stepwise manner from -0.05 V to 0.05 V with 10 different voltages in total. The voltage step was held for 2.5 min to allow the ionic current to relax in freshly prepared CT complex electrolytes, and for 30 min in treated electrolytes. The voltage hold duration was sufficient for reaching steady state. The plateau current at each voltage stage was then plotted as a function of voltage, and the slope of the line was taken as the electronic conductance.

Thermal annealing and water vapor treatment. Thermal annealing was performed at 130 °C for 30 min with a ramping up rate of 10 °C/min within the Quatro temperature control system under constant pressure. After being cooled down to room temperature, the coin cells were transferred into a humidity chamber for 7 hrs, where the relative humidity (RH) values were held at 95-99 %. Coin cells subjected to purposeful water vapor treatment were not crimped until this treatment was complete.

Wide-angle X-ray scattering (WAXS). The fresh and treated electrolytes were loaded into special glass capillary tubes with an outer diameter of 1.5 mm and sealed in an argon-filled glovebox to prevent ambient moisture from impacting the samples. WAXS measurements were conducted at Advanced Photon Source synchrotron beamline 12-ID-B, operated by the Chemical and Materials Science group at Argonne National Laboratory. An X-ray beam wavelength of 0.9322 Å (photon energy 13.3 eV) was used to take measurements. Temperature-dependent WAXS data was taken upon heating from 25, 100, 120, and 130 ℃. The temperature was ramped at 5 °C/min with 5 min of stabilization time at 25, 100, and 120 ℃ and 30 min at 130 ℃.

Karl Fischer (KF) titration. The determinations of water content in the electrolytes were conducted with a coulometric KF titrator (Mettler Toledo, C20). Anhydrous CH_3CN was dried over 3 Å molecular sieves in the glovebox before use. Then, 2.5 mg of CT electrolyte pellet was added into 3.5 mL anhydrous CH_3CN and stirred for 2 hrs to obtain a suspension. Subsequently, the water content in each electrolyte was measured three times.

Scanning electron microscopy/eenergy dispersive X-ray spectroscopy (SEM/EDS). Both fresh and treated electrolyte samples as well as pure CT complex samples recovered from coin cells were transferred onto carbon tapes in the glovebox and transported to the SEM facility via a PELCO vacuum pin stub holder to minimize ambient air exposure. SEM images were collected using a Magellan 400 FESEM coupled with a Bruker energy dispersive x-ray spectrometer for EDS measurements. The working distance was 4.5 mm, with a voltage of 10 kV and beam current of 25 pA.

Fourier transform infrared spectroscopy (FTIR). FTIR spectra of fresh and treated electrolytes were obtained using a Bruker Tensor 27 FTIR with a diamond lens Attenuated Total Reflectance (ATR) module. The measurements were conducted in a N_2 atmosphere to minimize ambient moisture content impact. The spectra were collected from 4000 cm^{-1} to 650 cm^{-1} at 4 cm^{-1} resolution with 64 scans.

Impedance measurements and equivalent circuit fitting for ionic, electronic, and interparticle conductivity. CT complex electrolytes, containing both ionic and electronic conducting carriers, can be considered as mixed conductors of different degrees, whether they are predominantly electronically conducting or mostly ionically conducting. EIS was used to decouple the ionic and electronic components of resistances in the electrolyte using a coin cell setup where the solid-state electrolyte was sandwiched with two stainless steels as electrodes and donut-shaped Teflon film as the spacer. In such a configuration,

the ions were conducted through the electrolyte and blocked at the electrolyte/electrode interface whereas the transport of electrons was not blocked at the interface.[3] From the impedance expressions of these elements listed below, the frequency-dependent impedance of the proposed equivalent model can be calculated based on elementary circuit theory. CPEs were used here to account for inhomogeneous or imperfect capacitance, and were represented by the parameters Q, α, β, and γ , where Q was a pseudocapacitance value, and α, β, and γ meant their deviation from ideal capacitive behaviors.

Impedance expression of each component:

$$Z_c = R_c$$

$$Z_e = R_e$$

$$Z_i = R_i$$

$$Z_{int} = R_{int}$$

$$Z_{CPE_{dl}} = \frac{1}{Q_{dl}(j2\pi f)^{\beta}}$$

$$Z_{CPE_g} = \frac{1}{Q_g(j2\pi f)^{\alpha}}$$

$$Z_{CPE_{int}} = \frac{1}{Q_{int}(j2\pi f)^{\gamma}}$$

Total impedance expression:

$$Z = Z_c + \frac{1}{\frac{1}{Z_{CPE_g}} + \frac{1}{Z_e} + \frac{1}{Z_i + Z_{CPE_{dl}} + \frac{1}{\frac{1}{Z_{int}} + \frac{1}{Z_{CPE_{int}}}}}}$$

$$= R_c + \frac{1}{Q_g(j2\pi f)^{\alpha} + \frac{1}{R_e} + \frac{1}{R_i + \frac{1}{Q_{dl}(j2\pi f)^{\beta}} + \frac{1}{\frac{1}{R_{int}} + \frac{1}{Q_{int}(j2\pi f)^{\gamma}}}}}$$

When using AC mode in EIS measurements, the expression of total impedance Z can be separated into two variables, Z_{re} and Z_{im}, both of which can be plotted in the Nyquist plot, with Z_{re} as the x-axis and $-Z_{im}$ as the y-axis. Typically, a pure electronic or ionic conduction displays one semi-circle shape in the Nyquist plot. However, in a mixed ionic-electronic conductor, it is expected to have two semicircles, which are indicative of two different time constants, one associated with ionic conduction at the higher frequencies and the other relevant to electronic conduction at the low-frequency range.[4] In our mixed-conducting electrolyte, the initial guess of electronic resistance was derived from the low-frequency impedance obtained using the AC impedance mode, and later the ionic, electronic, and interparticle resistances were fitted from the corresponding Nyquist plot using the impedance expression formula.

Thermal Characterization:

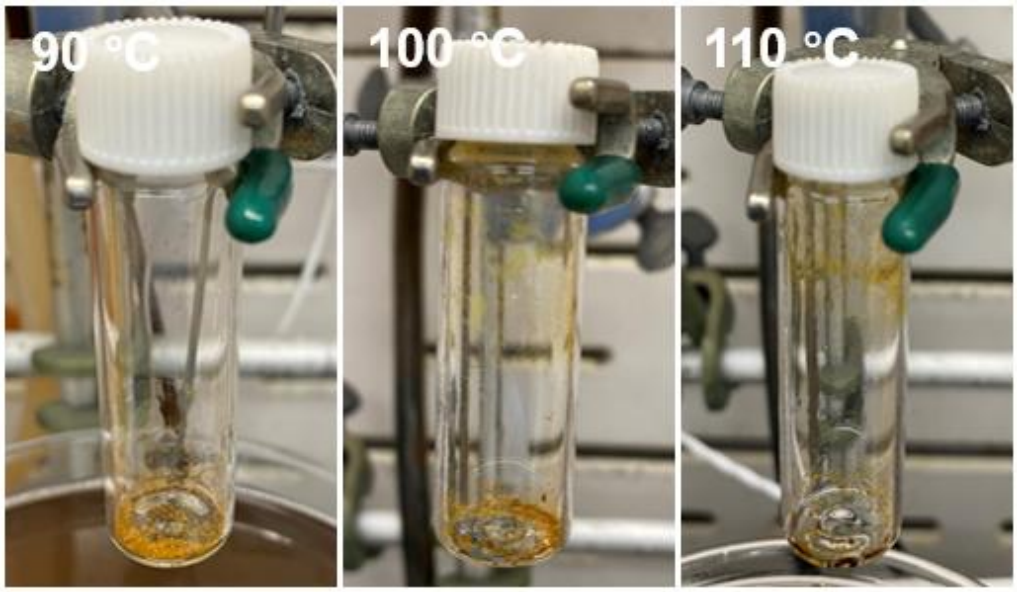

Figure S1. The images when TTF was heated up to melt at 120 °C in an oil bath. TTF started to sublime before the temperature reached 120 °C. From left to right: 90, 100, and 110 °C.

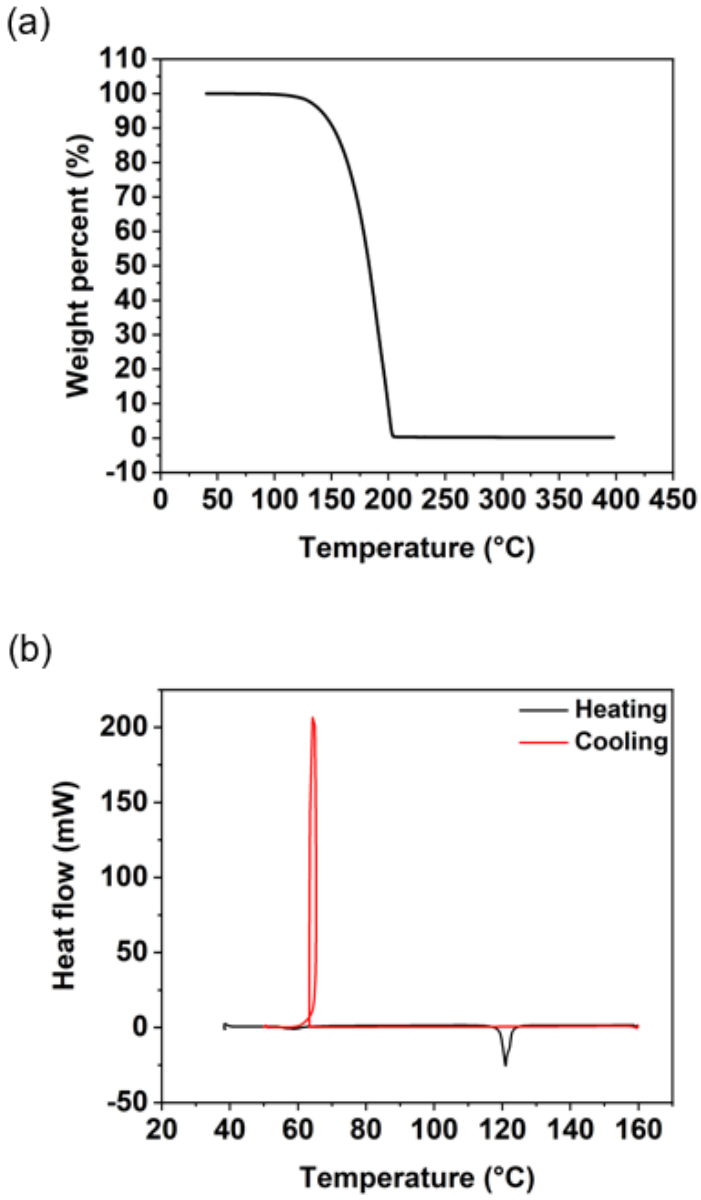

Figure S2. (a) TGA thermogram of TTF. (b) DSC thermograms of TTF for the second heating run. TTF is a sublimable compound which starts to sublime at around 110 °C with a melting temperature at 120 °C. Therefore, in our work, to prevent the sublimation at higher temperatures, a solution mixing method was adopted to fabricate the neat CT complex and electrolytes.

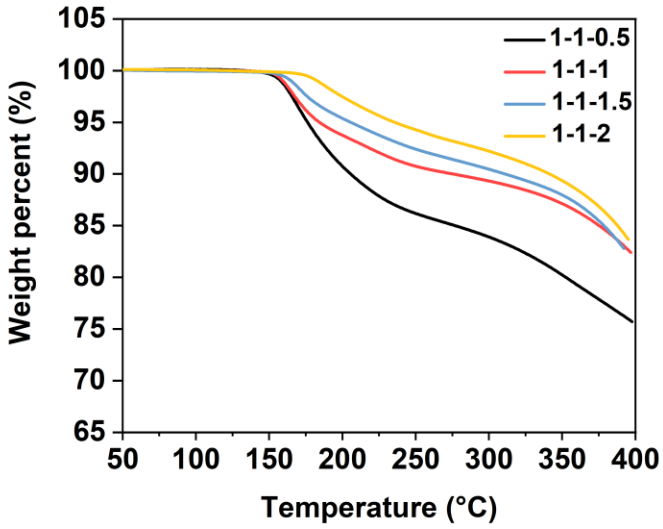

Figure S3. TGA thermogram of all four fresh electrolytes at a ramp rate of 5 °C/min. The weight loss of 0.5% occurred at temperatures 152, 155, 158, and 173 °C for electrolytes 1-1-0.5, 1-1-1, 1-1-1.5, and 1-1-2, respectively.

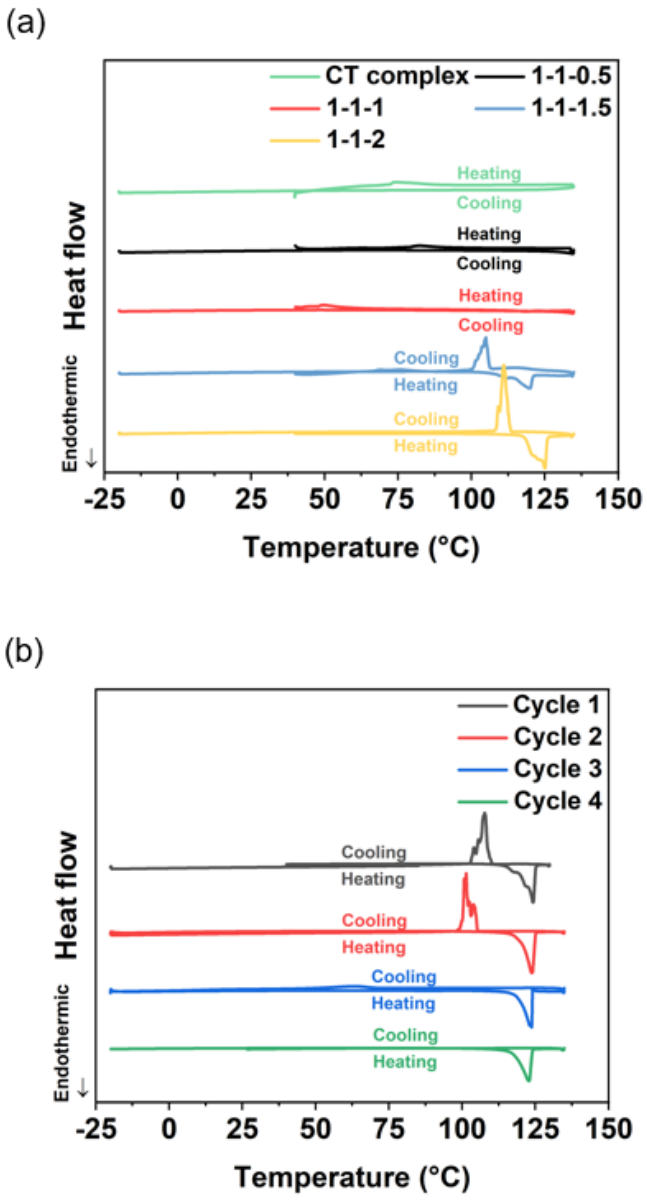

Figure S4. (a) DSC thermograms of fresh CT complex and electrolytes on first heating and cooling scans at a rate of 5 °C/min. The exothermic peaks on heating scans in CT complex, 1-1-0.5 and 1-1-2 were cold crystallization, because samples were taken out from the hot vacuum oven in the glovebox after drying to prevent potential residual solvent trapping. The endothermic peaks on heating and exothermic peaks on cooling in 1-1-1.5 and 1-1-2 can be ascribed to the CT complex crystal breaking up and partial dissolution of LiTFSI at (203) and (210) orientation, which was consistent with the WAXS profiles in **Figure S17**. (b) DSC thermograms of fresh 1-1-2. The electrolyte was held at 130 °C for 30 min at cycle 1 and at 135 °C for 2 min to in other cycles. The endothermic and exothermic peaks gradually shifted to lower temperatures, and disappeared on the cooling run at cycle 4.

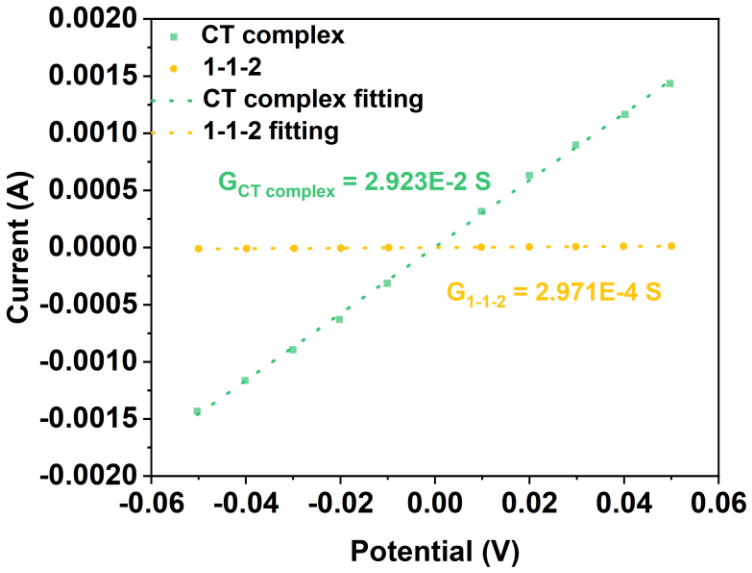

Figure S5. The DC polarization measurement used to determine the electronic conductivity at 25 °C (**Figure 1d**). Both potential and current were read from the plateau of each stage. The fitted slope represented the electronic conductance. The electronic conductivity was calculated from $\sigma = GL/A$, where G was conductance, L was the electrolyte thickness, and A was the cross-sectional area. The electronic conductivity of CT complex and 1-1-2 tested from DC polarization were 1.05×10^{-3} and 1.07×10^{-5} S/cm, respectively.

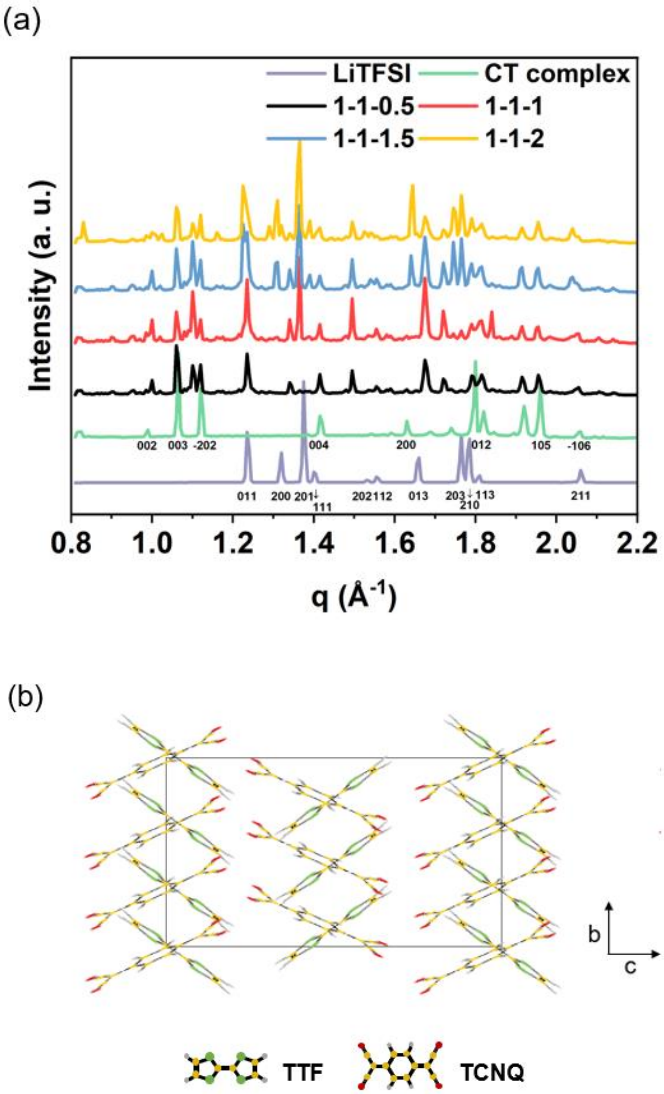

Figure S6. (a) WAXS data of pure TTF-TCNQ CT complex, neat LiTFSI, electrolyte 1-1-0.5, 1-1-1, 1-1-1.5 and 1-1-2 powder. (b) Orthogonal view of the molecular structure of TTF-TCNQ CT complex along the direction perpendicular to the (bc)-plane of TTF-TCNQ (LiTFSI not shown).

In organic electronic conductors, the electronic conductivity is largely influenced by the arrangements of crystals. Typically, the segregated stacking of TTF and TCNQ usually results in higher electronic conductivity compared with the mixed stacked structures.[5] Hence, the crystalline structure of the CT mixtures was characterized via WAXS. **Figure S6a** shows the WAXS pattern of LiTFSI (commercial product after drying), pure CT complex, and mixtures with different compositions. It was revealed that the CT complex had a segregated packing in which TTF and TCNQ held a face-to-face configuration within the same molecules (**Figure S6b**).[6,7] In such a segregated stacking geometry, an unpaired electron would hop from one molecule to the adjacent molecule. As the molecular potential of the same molecules was similar, the electronic conduction along the stacking direction would not be limited,[5] whereas there would be a large activation energy barrier for conduction in the mixed stacking compounds, and that was why the fabricated CT complex had such a high electronic conductivity at 10^{-3} S/cm at room temperature.

Upon the addition of lithium salt, characteristic peaks of pristine LiTFSI were still present in the WAXS profile, even in electrolyte 1-1-0.5 which had the least amount of LiTFSI. When LiTFSI was not the dominant part in the electrolytes (electrolytes 1-1-0.5 and 1-1-1), the disappearance of the peak at q = 1.32 Å in LiTFSI indicated a decrease in crystallinity at a certain orientation. Nevertheless, three new peaks emerged at q = 1.1, 1.34, and 1.5 $Å^{-1}$, which align with reflections from crystalline LiTFSI-water complexes (**Figure S18**). This data indicates that the fresh mixtures contain a small but non-negligible amount of water, however this water does not facilitate practical ionic conductivity.

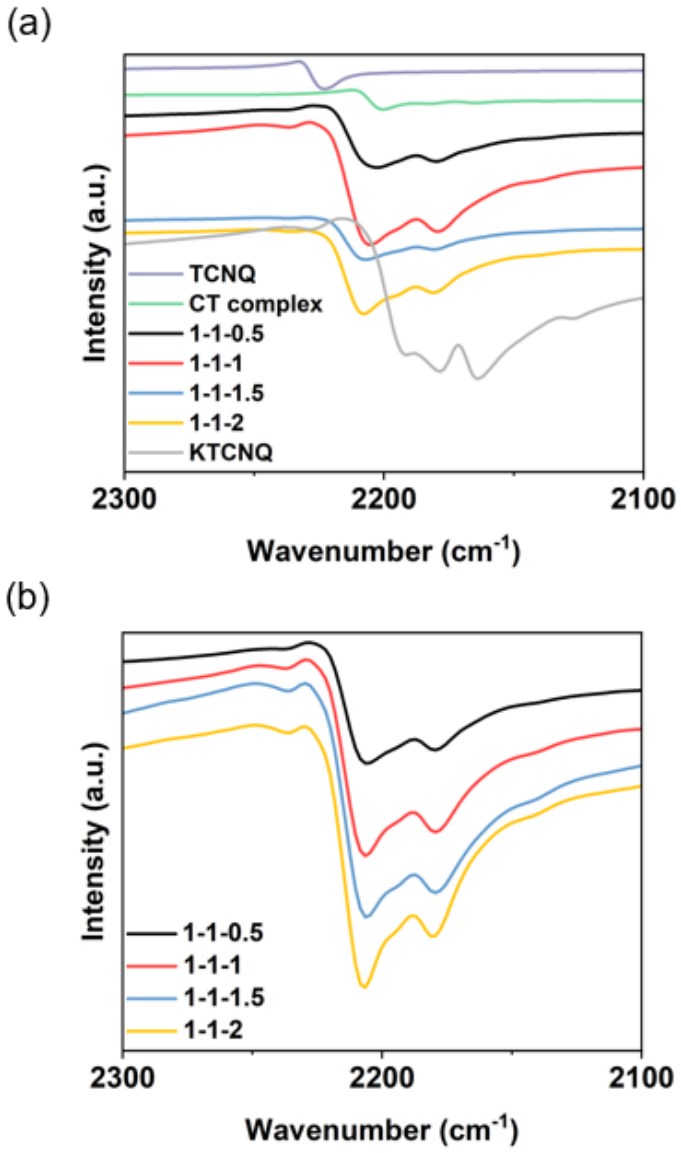

Figure S7. (a) FTIR spectra of fresh CT complex electrolytes as well as pure TCNQ (neutral compound), CT complex, and KTCNQ (anion compound). (b) FTIR spectra of treated CT complex electrolytes.

The degree of charge transfer (DCT) represents the ability of charge transfer between the electron donors and acceptors, and correlates the structure to the properties of the donor-acceptor complexes. One common method used to evaluate DCT is based on the wavenumber change of certain vibrational modes in FTIR before and after charge transfer. DCT can be calculated via the following equation:

$$\mathrm{DCT} = \frac{2\Delta v}{v_0} \times \frac{1}{1-\frac{{v_1}^2}{{v_0}^2}}$$

where $\Delta v = v_0 - v_{CT}$, v_0, v_1, and v_{CT} represent the asymmetric cyano group (-C≡N) stretching wavenumbers in neutral (TCNQ), anion (KTCNQ), and partially charge transferred states (CT complex and electrolytes), respectively.[8,9]

In the fresh samples, peaks ranging from 2183 to 2222 cm^{-1} represent the -C≡N stretching mode in TCNQ with different states. Three characteristic vibrational peaks specific to 2192, 2183, and 2164 cm^{-1} corresponding to the -C≡N stretching mode can be assigned to the anion state of $TCNQ^-$ in the salt KTCNQ.[10] There was only one -C≡N vibrational peak at 2200 cm^{-1} in CT complex, but two peaks in fresh electrolytes (one at the range of higher than 2200 cm^{-1}, and one at around 2183 cm^{-1}). As this peak was not observed in pure CT complex, it was reasonable to attribute it to the interaction between Li^+ and -C≡N group of TCNQ, similar to the ionic state in salt KTCNQ. The -C≡N vibrational peaks at 2200 cm^{-1} and 2183 cm^{-1} meant the partially charge transferred states and ionic states. Therefore, in addition to the crystalline doped state of LiTFSI in the electrolytes, there was also a partial amount of ioion-solvatedi$^+$ and $TFSI^-$. After thermal annealing and water vapor treatment, the wavenumbers of two peaks belonging to the -C≡N group did not change obviously, which showed that its local environment kept very similar.

Table S1. Degree of charge transfer (DCT) analysis of fresh TCNQ, KTCNQ, and CT complex, as well as fresh and treated electrolytes. The peak wavenumbers shown below were from the -C≡N stretching mode at the higher wavenumber range (2200 cm^{-1} and higher), representing the partially charge transferred states.

		TCNQ	KTCNQ	CT complex	1-1-0.5	1-1-1	1-1-1.5	1-1-2
Wavenumber (cm^{-1})	Fresh	2222	2183	2200	2202	2205	2207	2208
	Treated	-	-	-	2205	2207	2208	2209
DCT	Fresh	-	-	0.57	0.52	0.44	0.38	0.36
	Treated	-	-	-	0.44	0.38	0.36	0.34

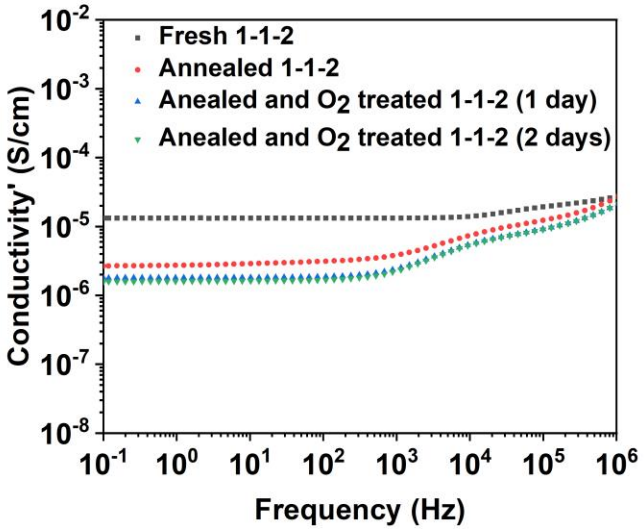

Figure S8. The AC conductivity of electrolyte 1-1-2 at the fresh, thermally annealed, and pure O_2 treated states at room temperature.

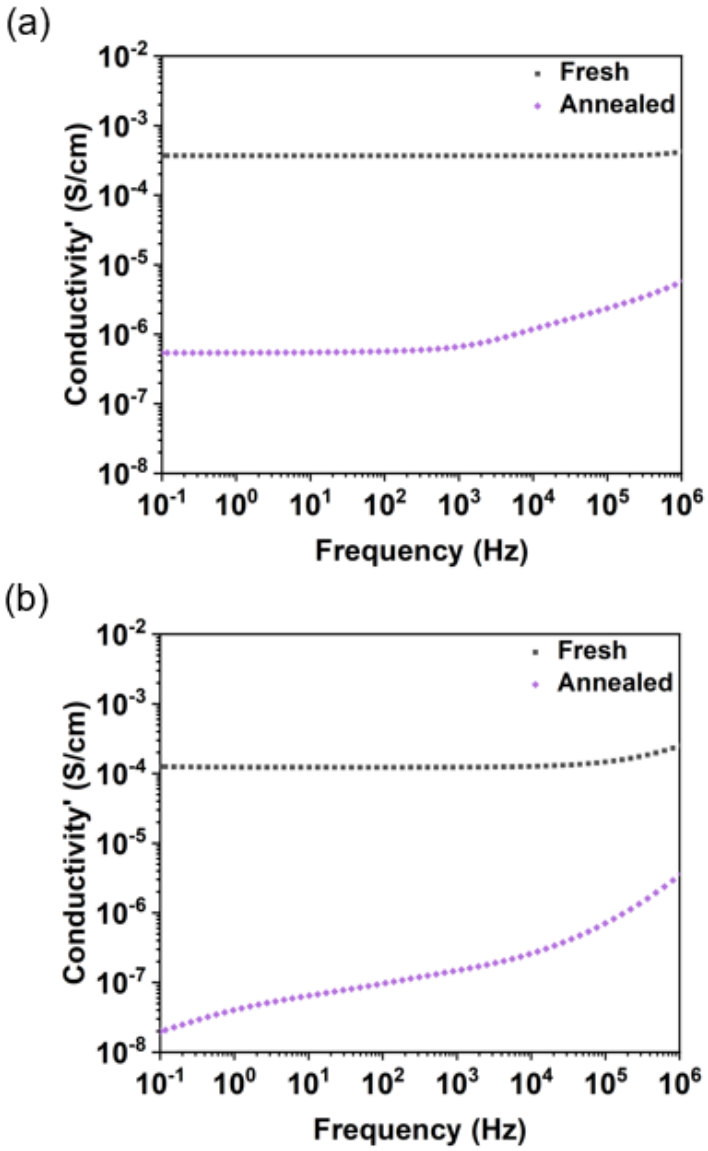

Figure S9. Room-temperature AC conductivity profiles of wet fresh and thermally annealed electrolyte 1-1-2 with different amounts of liquid water added purposefully prior to coin cell assembly. The molality of LiTFSI in water was 40 m (a) and 80 m (b).

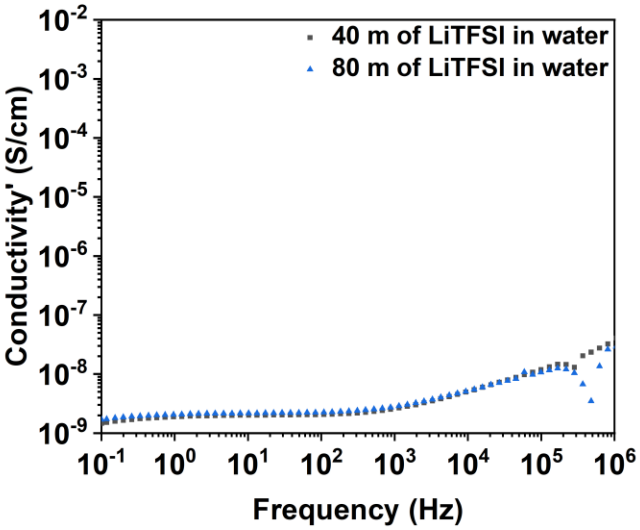

Figure S10. Room-temperature AC conductivity profiles of LiTFSI with different amounts of water.

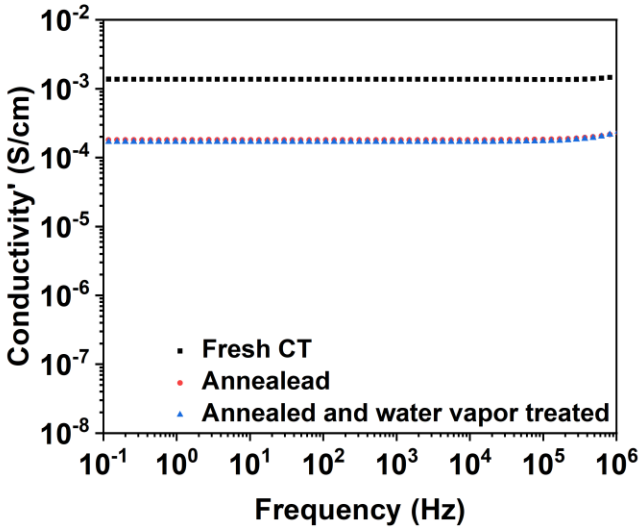

Figure S11. Room-temperature AC conductivity profiles of freshly prepared CT complex (black); annealed CT complex after being cooled down (red); and annealed CT complex after being treated with water vapor at 95-99 %RH for 7 hrs (blue). Thermal annealing decreased the electronic conductivity of pure CT complex, but water vapor did not have any impact.

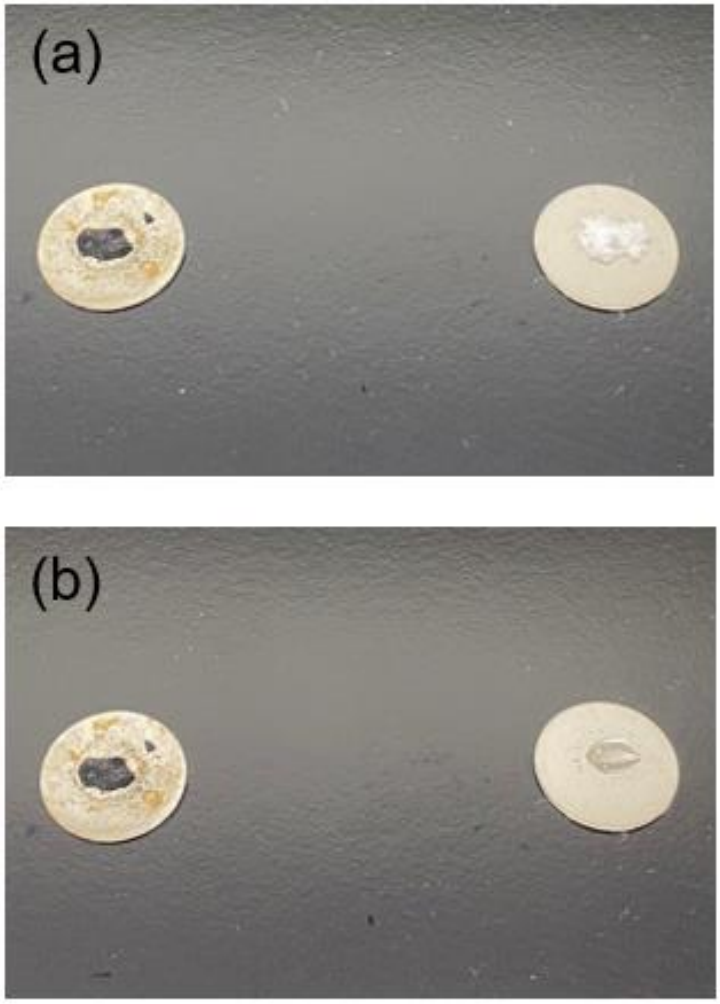

Figure S12. The comparison of electrolyte 1-1-2 and pure LiTFSI exposed in ambient air with a 26% RH after 1 hr: (a) before and (b) after.

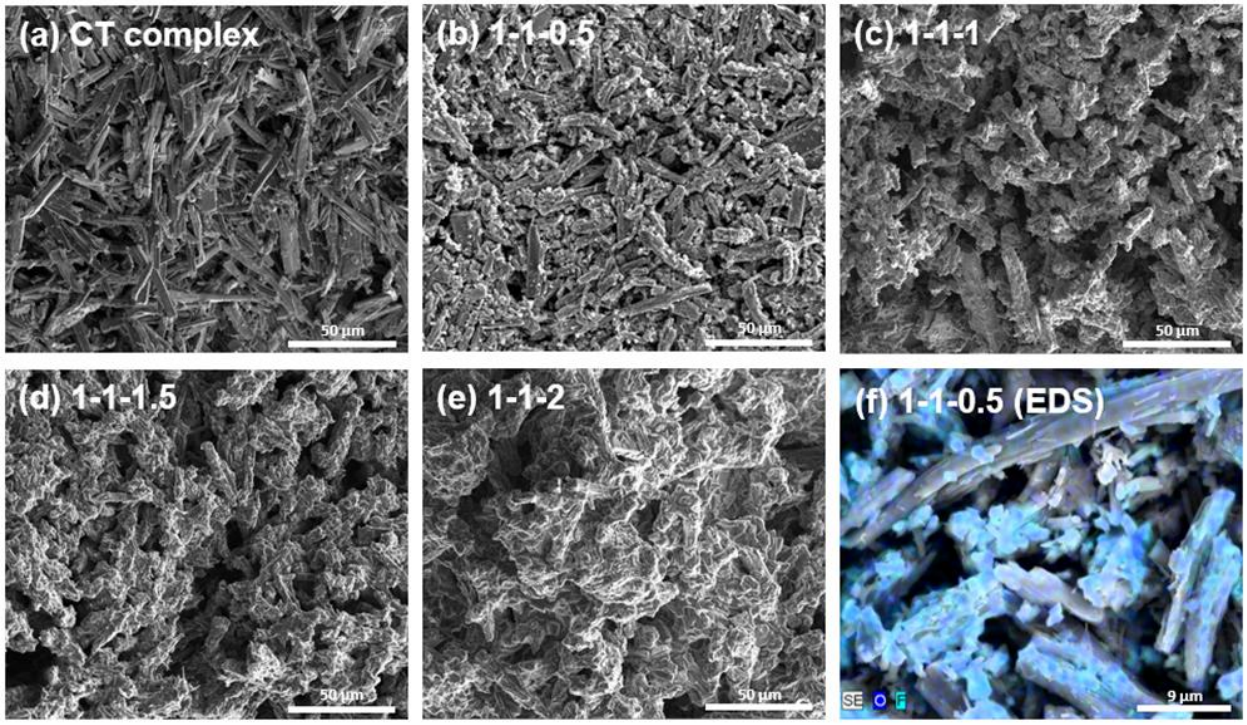

Figure S13. SEM images of the fresh samples: (a) CT complex; (b) 1-1-0.5; (c) 1-1-1; (d) 1-1-1.5; (e) 1-1-2, and (f) EDS mapping of 1-1-0.5, where elements oxygen and fluorine only come from LiTFSI.

The pure CT complex had regular needle-like shapes with a typical width of 2-3 um. When the doping level of LiTFSI increased, the obtained solid-state electrolytes were more like irregular rods with inhomogeneous surfaces as well as larger width sizes, where in electrolyte 1-1-2, the width of rods were around 5 um. It was also visible that some percolated network started to form with more addition of lithium salt. Elemental mapping of electrolyte 1-1-0.5 (**Figure S13f**) clearly illustrated that there were oxygen- and fluorine-rich particle clusters which may be ascribed to LiTFSI crystals.

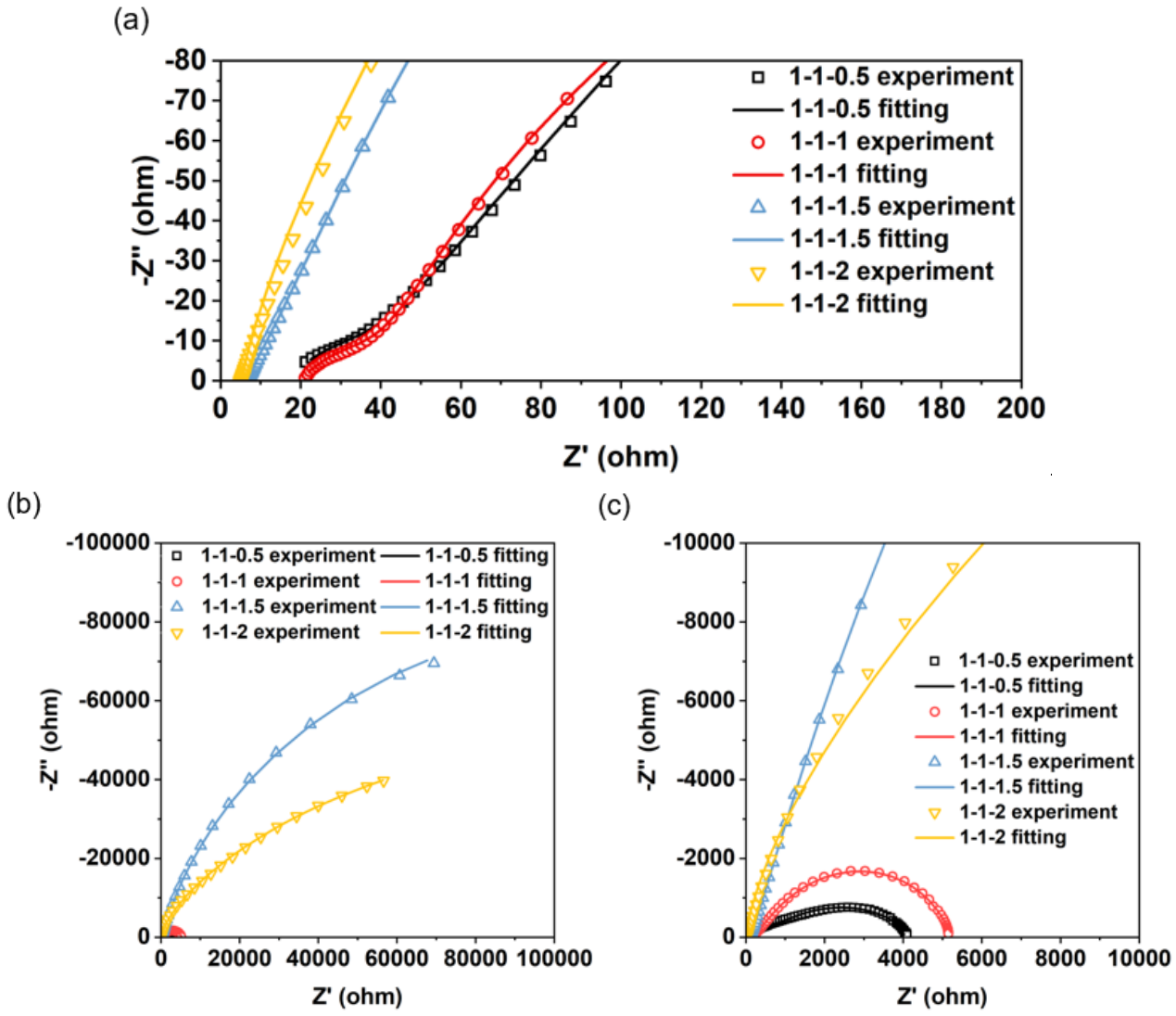

Figure S14. The experimental data (points) and equivalent circuit model fitting lines for all four treated electrolytes at 100 °C (b, zoomed-in plot of **Figure 4b**) and 25 °C (b) and (c, zoomed-in plot).

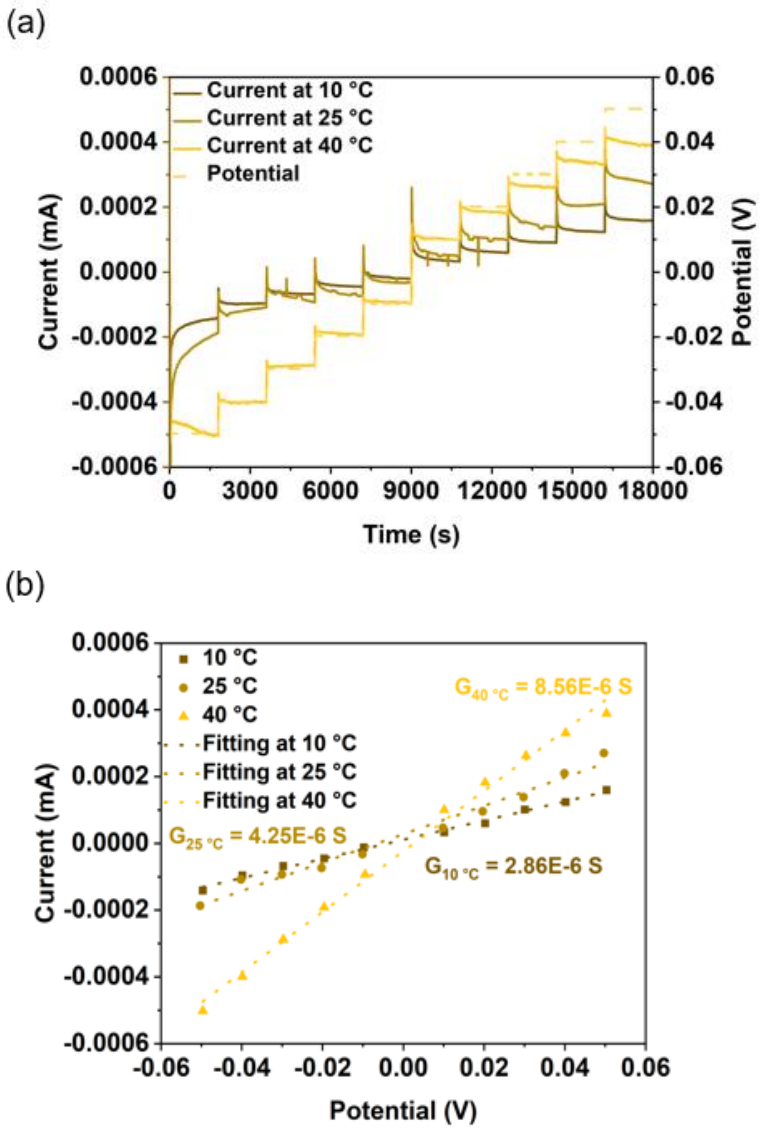

Figure S15. DC polarization profile (a) and current-potential slope fitting (b) of treated electrolyte 1-1-2 at 10, 25, and 40 °C. The electronic conductivity of treated electrolyte 1-1-2 tested from DC polarization were 1.03×10^{-7}, $1.53 \times 10^{-7,}$ and 3.08×10^{-7} S/cm at 10, 25, and 40 °C respectively.

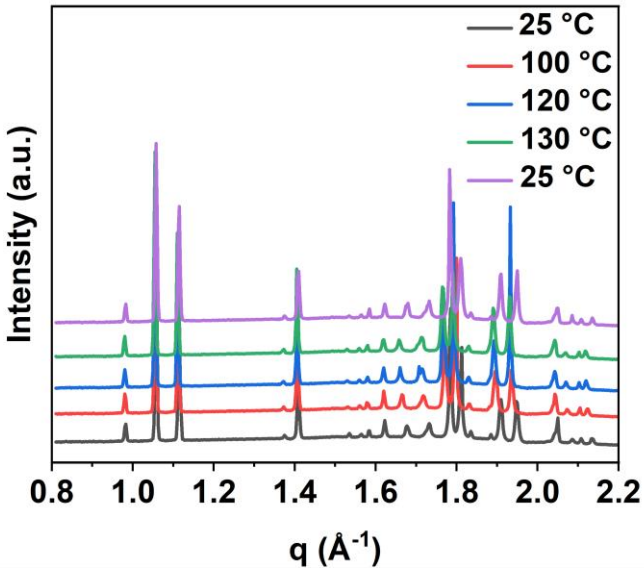

Figure S16. Temperature-dependent WAXS profile of pure CT complex. WAXS data was collected at temperatures from 25 to 130 °C with a ramp rate of 5 °C/min and stabilization of 5 min, except for a longer equilibration time at 130 °C of 30 min. Then the temperature was ramped down to 25 °C with the same rate and equilibrium time (purple).

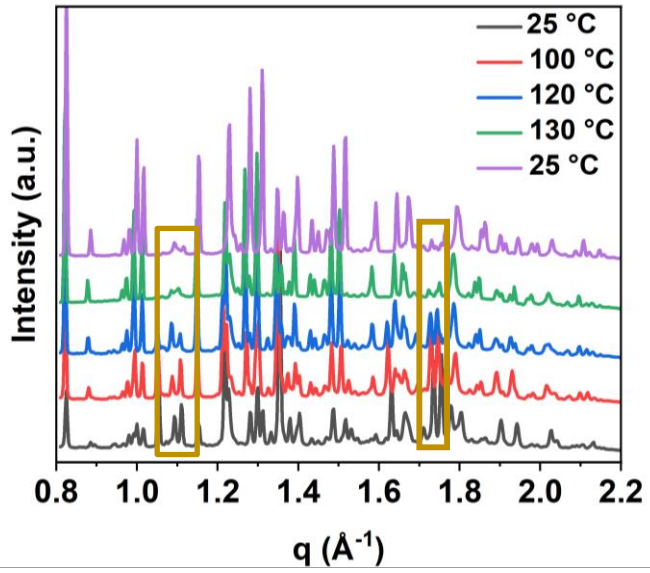

Figure S17. Temperature-dependent WAXS profile of fresh electrolyte 1-1-2. WAXS data was collected at a temperature from 25 to 130 °C with a ramp rate of 10 °C/min and stabilization of 5 min, except for a longer equilibration time at 130 °C of 30 min. Then the temperature was ramped down to 25 °C with the same rate (purple). The boxes highlight areas of the profiles with significant changes that are not explained by additive effects. We believe that the disappearances of peak at q = 1.065 and 1.12 $Å^{-1}$ when heating from 120 to 130 °C represents disorder of the center axis planes between TTF and TCNQ stacks.[6] Another peak originating from LiTFSI at q = 1.765 $Å^{-1}$ disappeared, which indicates that the LiTFSI lattice was disordered at the (203) and (210) direction in thermal annealing.[11]

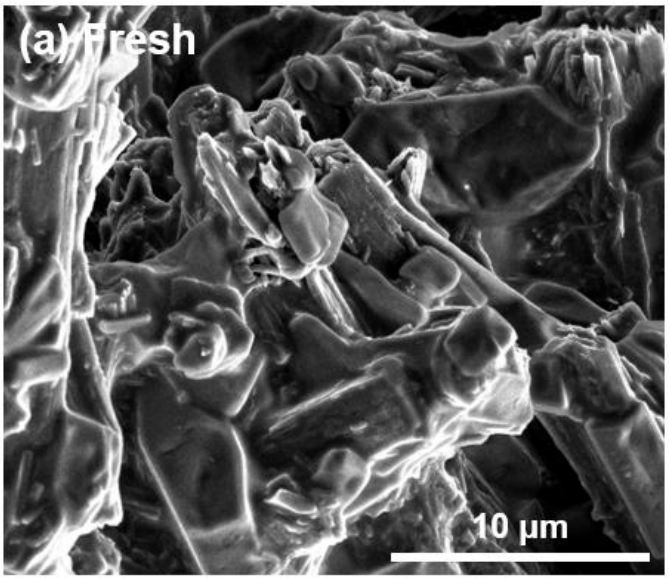

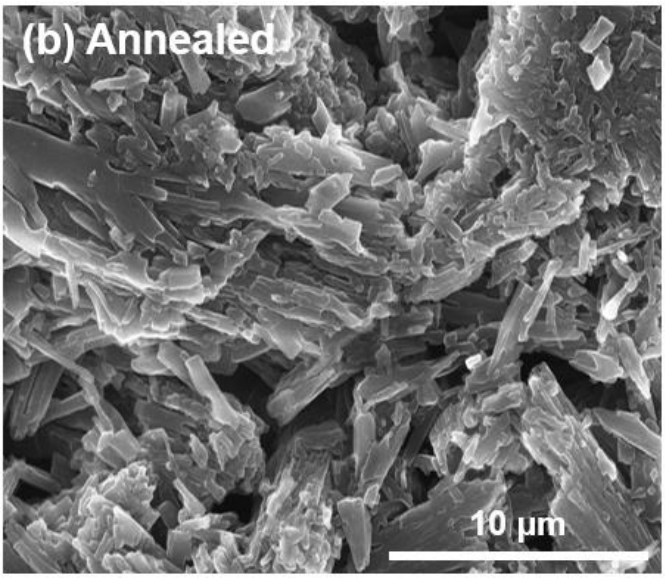

Figure S18. SEM images of electrolyte 1-1-2, focused on CT complex-rich phase, in the fresh state (a) and treated state (b). The CT particle sizes decreased and particle shapes became irregular.

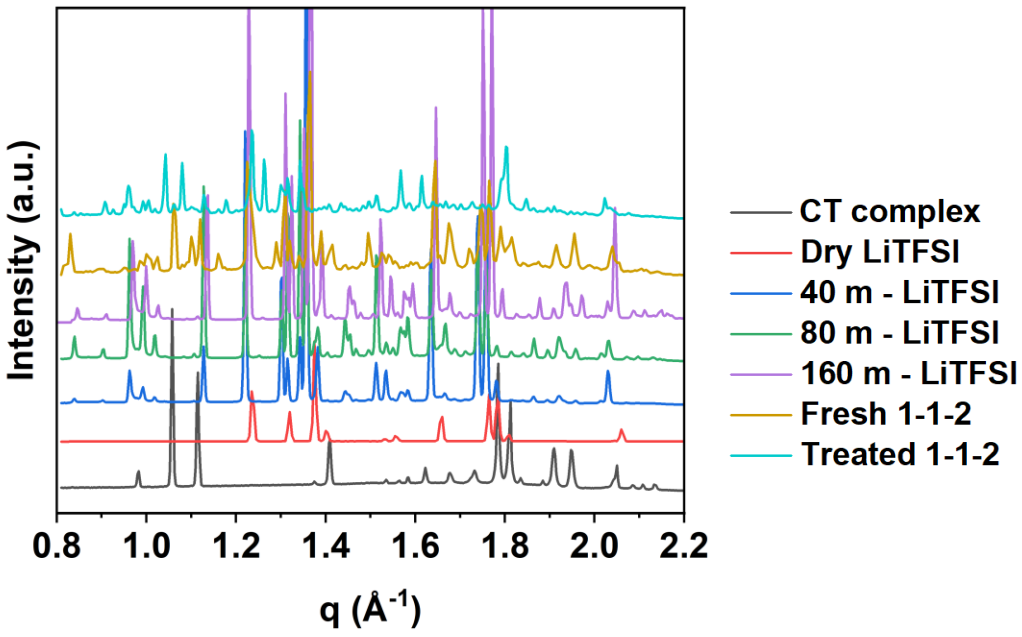

Figure S18. Room temperature WAXS profiles of fresh and treated electrolyte 1-1-2. Data of pure CT complex and LiTFSI with different amounts of water (the molality of LiTFSI in water were 40, 80, and 160 m) as a reference. The treated electrolyte profile contains key differences from the fresh mixture profile, including both peak deletions and peak additions. These peak additions are not all observed in the profiles for wet LiTFSI, and further analysis is suggested in future work. Lower intensity of the treated profile suggests some amorphization.

Table S2. Water vapor content in all treated electrolytes by mass percent, mole fraction, and molality.

Sample	Water content by mass percent in the electrolyte (%)	Water content by mole fraction in the electrolyte	Molality of electrolytes in water (m; mol CT / kg H_2O)	Molality of LiTFSI in water (m; mol LiTFSI / kg H_2O)
1-1-0.5	0.65 ± 0.06	0.20 ± 0.02	280 ± 20	140 ± 10
1-1-1	0.81 ± 0.15	0.31 ± 0.06	180 ± 30	180 ± 30
1-1-1.5	0.82 ± 0.07	0.38 ± 0.03	150 ± 10	220 ± 20
1-1-2	0.83 ± 0.14	0.45 ± 0.08	120 ± 20	250 ± 40

References

(1) Wu, L.; Wu, F.; Sun, Q.; Shi, J.; Xie, A.; Zhu, X.; Dong, W. A TTF-TCNQ Complex: An Organic Charge-Transfer System with Extraordinary Electromagnetic Response Behavior. *J. Mater. Chem. C* **2021**, *9* (9), 3316–3323. https://doi.org/10.1039/d0tc05230b.

(2) Melby, L.R., Harder, R.J., Hertler, W.R., Mahler, W., Benson, R.E. and Mochel, W.E. (1962) Substituted Quinodimethans. II. Anion-Radical Derivatives and Complexes of 7,7,8,8-Tetracyanoquinodimethan. *Journal of the American Chemical Society*, **1962**, *84*, 3370-3374. https://doi.org/10.1021/ja00876a028

(3) Huggins, R. A. Simple Method to Determine Electronic Conductivity and Ionic Components of the Conductors in Mixed a Review. *Ionics (Kiel).* **2002**, *8* (3–4), 300–313. https://doi.org/10.1007/BF02376083.

(4) Feig, V. R.; Tran, H.; Lee, M.; Bao, Z. Mechanically Tunable Conductive Interpenetrating Network Hydrogels That Mimic the Elastic Moduli of Biological Tissue. *Nat. Commun.* **2018**, *9* (1), 1–9. https://doi.org/10.1038/s41467-018-05222-4.

(5) Torrance, J. B. An Overview of Organic Charge-Transfer Solids: Insulators, Metals, and the Neutral-Ionic Transition. *Mol. Cryst. Liq. Cryst.* **1985**, *126* (1), 55–67. https://doi.org/10.1080/15421408508084154.

(6) Kistenmacher, T. J.; Phillips, T. E.; Cowan, D. O. The Crystal Structure of the 1:1 Radical Cation–Radical Anion Salt of 2,2'-Bis-l,3-Dithiole (TTF) and 7,7,8,8-Tetracyanoquinodimethane (TCNQ). *Acta Crystallogr. Sect. B Struct. Crystallogr. Cryst. Chem.* **1974**, *30* (3), 763–768. https://doi.org/10.1107/s0567740874003669.

(7) Goudappagouda; Chithiravel, S.; Krishnamoorthy, K.; Gosavi, S. W.; Santhosh Babu, S. Seeded On-Surface Supramolecular Growth for Large Area Conductive Donor-Acceptor Assembly. *Chem. Commun.* **2015**, *51* (52), 10439–10442. https://doi.org/10.1039/c5cc03091a.

(8) Iguchi, H.; Furutani, H.; Kimizuka, N. Ionic Charge-Transfer Liquid Crystals Formed by Alternating Supramolecular Copolymerization of Liquid π-Donors and TCNQ. *Front. Chem.* **2021**, *9* (March), 1–12. https://doi.org/10.3389/fchem.2021.657246.

(9) Dar, A. A.; Rashid, S. Organic Co-Crystal Semiconductors: A Crystal Engineering Perspective. *CrystEngComm* **2021**, *23* (46), 8007–8026. https://doi.org/10.1039/d1ce01117k.

(10) Ramanathan, R.; Kandjani, A. E.; Walia, S.; Balendhran, S.; Bhargava, S. K.; Kalantar-Zadeh, K.; Bansal, V. 3-D Nanorod Arrays of Metal-Organic KTCNQ Semiconductor on Textiles for Flexible Organic Electronics. *RSC Adv.* **2013**, *3* (39), 17654–17658. https://doi.org/10.1039/c3ra43291b.

(11) Nowinski, J. L.; Lightfoot, P.; Bruce, P. G. Structure of LiN(CF3SO2)2, a Novel Salt for Electrochemistry. *J. Mater. Chem.* **1994**, *4* (10), 1579–1580. https://doi.org/10.1039/JM9940401579.